Training Data Selection and Update for Airborne Post-Doppler Space-Time Adaptive Processing

André B. C. da Silva, Stefan V. Baumgartner
German Aerospace Center (DLR), Microwaves and Radar Institute, Oberpfaffenhofen, Germany
E-mail: andre.silva@dlr.de

Abstract

The training data selection and update are crucial steps for the space-time adaptive processing (STAP) operation, since contaminated training data result in a decreased clutter suppression performance, an incorrect constant false alarm rate (CFAR) threshold and target cancellation by self-whitening. This paper presents a promising algorithm that selects the training data by applying a moving window, taking into account the changes of the clutter statistics over space and time. The goal is to improve the clutter suppression capability and, thus, to increase the number of true detections. The benefits of the proposed algorithm are verified using real 4-channel X-band radar data acquired by the DLR's airborne F-SAR.

1 Introduction

The clutter covariance matrix (CCM) estimation is an essential step of space-time adaptive processing (STAP) algorithms, since the interference spectral properties are rarely known in practice and must be estimated using training data. However, in reality the training data are frequently contaminated by discrete scatterers and interfering targets, resulting in an incorrect CCM estimation and threshold setting that can cause target cancellation. Therefore, the selection of the training data plays an important role for the STAP operation [1-2].

An interesting literature review about training data selection methods is presented in [3]. However, several of the discussed algorithms are time-consuming (e.g., designed for joint-domain STAP, which requires more sample support and processing time) or may require a massively complex series of decisions to be made in real-time, which is especially the case of knowledge-aided (KA) algorithms [4-5].

Training data selection and STAP processing are even more challenging when the aircraft is equipped with a low-cost fixed-mounted antenna array which does not allow the zero-Doppler beam steering. In this case, the time-varying acquisition geometry has to be considered during processing in order to obtain accurate detection, position and velocity estimation results.

Exemplarily, **Figure 1a** shows an F-SAR image of the Memmingen area in Germany (area on ground: 9.4 x 1.8 km^2). As it can be seen in **Figure 1b**, atmospheric turbulences result in time-varying changes of the yaw, pitch and roll angles of the aircraft. **Figure 1c** shows the change of the Doppler centroid (and therefore the antenna pointing), especially due to the yaw and pitch angles of the aircraft. **Figure 1d** shows the change of the texture (estimated using the heterogeneous clutter model presented in [6]) over time and slant range.

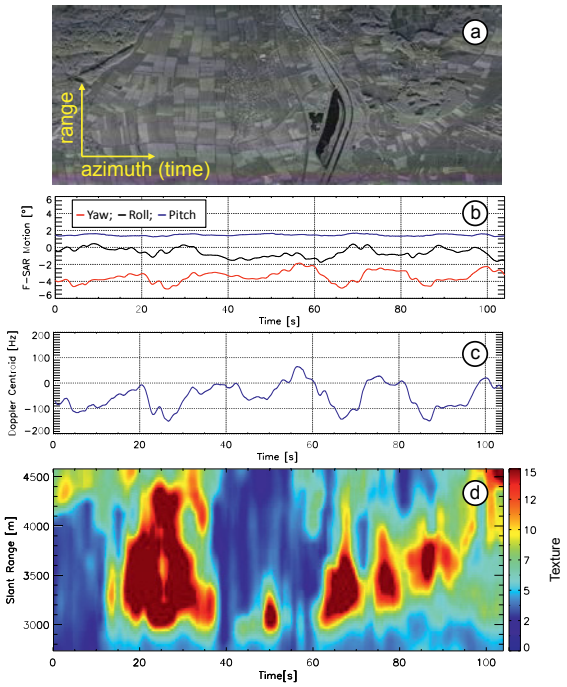

Figure 1: Examples of real-world problems on F-SAR data acquisition: (a) SAR image, (b) change of the yaw, pitch and roll angles, (c) change of the average Doppler centroid over time, and (d) change of the texture over time and slant range.

To combat the real-world problems shown in **Figure 1**, the training data must be updated regularly in order to reduce the errors in the estimated parameters of the STAP detections and, besides, to take into account potential changes in the clutter statistics.

This paper presents a promising algorithm for training data selection that can be applied on two ground moving target indication (GMTI) processors: the post-Doppler (PD) STAP-only and the PD STAP with road map in-

ISBN 978-3-8007-4636-1 / ISSN 2197-4403

formation [7-8]. The goal is to improve the clutter suppression capability and, thus, to increase the number of true detections. The proposed algorithm is evaluated using real 4-channel aperture switching data acquired by the DLR's airborne F-SAR [9].

2 Training Data Selection

This section describes two algorithms for selecting the training data for the CCM estimation: algorithm 1 is an example of a conventional method employed for PD STAP (used as reference) and algorithm 2 is novel. In both cases, the CCM is estimated according to [1]:

$$\widehat{\boldsymbol{R}}_{\mathrm{W}}(f_a) = \frac{1}{K}\sum_{k=1}^{K} \boldsymbol{z}(r_{\mathrm{k}}, f_{\mathrm{a}})\boldsymbol{z}^{H}(r_{\mathrm{k}}, f_{\mathrm{a}})\,, \qquad (1)$$

where f_{a} is the Doppler frequency, K is the number of range bins used for averaging, $(\cdot)^H$ is the Hermitian operator and $\boldsymbol{z}(r_{\mathrm{k}}, f_{\mathrm{a}})$ is the multi-channel data generally composed of:

$$\boldsymbol{z} = \boldsymbol{s} + \boldsymbol{c} + \boldsymbol{n} + \boldsymbol{j}\,, \qquad (2)$$

where $\boldsymbol{s}$ is the vector of the target signal, $\boldsymbol{c}$ the clutter, $\boldsymbol{n}$ the noise and $\boldsymbol{j}$ a possible jammer signal. For the CCM estimation, it is important to note that the multi-channel vectors $\boldsymbol{z}$ are almost free of strong discrete scatterers and moving target signals. This condition has to be ensured by a proper training data selection algorithm.

2.1 Algorithm 1 (Reference)

The principle of this algorithm is shown in **Figure 2**. In this case, the CCM is estimated only once per coherent processing interval (CPI), using all the samples of the CPI as training data (cf. red box in **Figure 2**). The main steps of this algorithm are listed below:

1. Obtain the CPI by segmenting the multi-channel data in time domain (e.g., by using 128 azimuth samples). Use all the available range samples n_{r};
2. Obtain the training data by using the full content of the CPI. Then, transform the training data to range-Doppler domain via an azimuth FFT;
3. Estimate the CCM for each Doppler frequency f_{a} according to (1), using $K = K_1 = n_{\mathrm{r}}$ range bins;
4. Apply the PD STAP processor on the CPI and estimate the CFAR threshold (according to [6]);
5. Detect the moving targets applying the CFAR threshold, then estimate their positions and line-of-sight velocities (using the equations in [1]).

It is pointed out that this algorithm does not perform data selection, since the full CPI is used as training data.

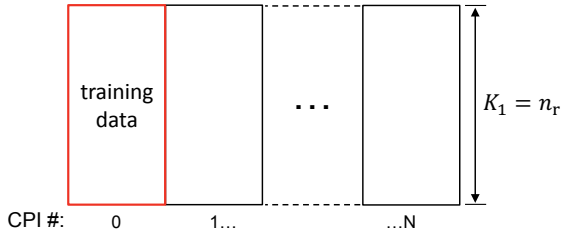

Figure 2: Principle of algorithm 1 (reference). The training data (red box) are obtained by using all samples of the CPI. The CCM is estimated only once per CPI.

2.2 Algorithm 2 (Novel)

The principle of this algorithm is shown in **Figure 3**. This algorithm applies a moving window over range and azimuth, where the training data (cf. red box in **Figure 3**) contain $L = 2T + D$ truncated CPIs with n'_{r} range bins. The CPIs marked as D (blue box) are processed by the PD STAP, while the adjacent CPIs marked as T are used only as training data.

The training data are built by: 1) "stacking" the L CPIs in time domain and 2) transforming the data to range-Doppler domain via an azimuth FFT (cf. detail in **Figure 3**). Thus, the training data have $K = n'_{\mathrm{r}}L$ available range bins. The main steps of this algorithm are listed below:

1. Select the data patch using L CPIs and n'_{r} range bins by segmenting the multi-channel data in time domain;
2. Build the training data by "stacking" the L CPIs;
3. Estimate the CCM for each Doppler frequency f_{a} according to (1), using $K = K_2 = n'_{\mathrm{r}}L$ range bins;
4. Apply the PD STAP processor on the training data and estimate the CFAR threshold;
5. Apply the PD STAP processor on the CPIs D and detect the moving targets using the CFAR threshold. Finally, estimate the positions and the line-of-sight velocities of the moving targets.

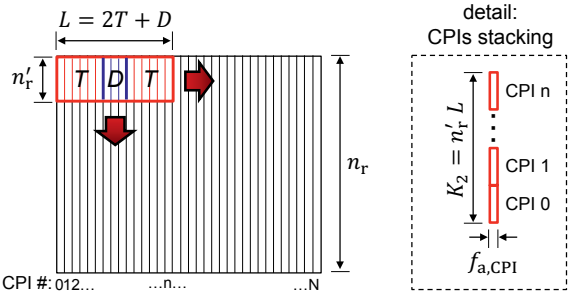

Figure 3: Principle of algorithm 2 (novel). The training data (red box) are updated as the window slides over range and azimuth. On the right, the detail shows the CPIs stacking technique for building the training data.

ISBN 978-3-8007-4636-1 / ISSN 2197-4403

3 Experimental Data

Both training data selection algorithms were tested using real 4-channel aperture switching data acquired by the DLR's airborne F-SAR. The flight campaign was conducted over the Allgäu airport in Memmingen in February 2007. **Figure 4** shows an optical image of the scene, where the cars 1-4 moved on the edges of the runway and car 5 moved off-road in circles. A detailed experiment description is found in [9-10]. The data take had 1024x16384 range-azimuth samples.

The positions and the velocities of the cars were known. The cars 1, 2 and 4 were equipped with radar reflectors in order to enhance their RCS and car 4 had a differential GPS (DGPS) receiver for retrieving reliable geographical reference positions and velocities.

The data were processed using CPIs of 1024x128 range-Doppler samples and the beamformers were applied using direction-of-arrival (DOA) angle steps of 0.05° within an interval determined by the azimuth antenna beam width. The probability of false alarm of the CFAR detector was set to $P_{fa} = 10^{-6}$.

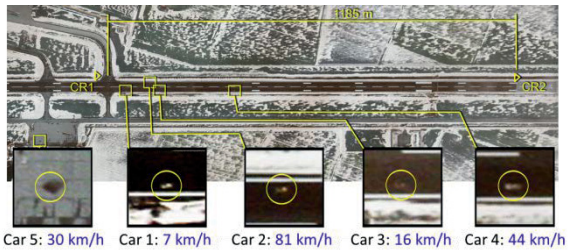

Figure 4: Optical image of the Allgäu airport in Memmingen. The cars 1-4 moved on the edges of the runway and car 5 moved off-road in circles [9-10].

3.1 Moving Window Length

The length of the moving window for algorithm 2 (i.e., the choice of the parameters D, T and n'_r) plays a big role for the STAP performance. Thus, in this subsection the impacts caused by different moving window lengths are shown and discussed using the experimental data. Two experiments were carried out, where the PD STAP with road map information [7-8] was used for counting the number of detections relocated to the runway.

3.1.1 Experiment 1: Parameters *D* and *T*

Figure 5a shows the number of true detections of cars 1-4 (i.e., $\text{True}_{\#1\text{-}4}$) as a function of the parameters D and T. In this case, all the available range bins were used (i.e., $n'_r = 1024$). Besides, the detections of car 5 were not counted since it moved off-road and thus its detections were discarded after applying the road map information. **Figure 5b** shows the number of false detections relocated to the runway as a function of the parameters D and T. In this case, the number of false detections was calculated by subtracting the number of relocated detections from the number of true detections ($\text{True}_{\#1\text{-}4}$).

For instance, a good compromise can be achieved when $D = 15$ and $T = 12$, where 450 true detections and only 2 false detections were obtained. Therefore, these parameters were chosen for the moving window applied on algorithm 2, so that $L = 2T + D = 39$ CPIs (nearly two seconds of data).

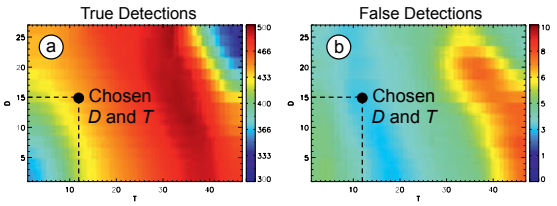

Figure 5: Number of detections relocated to runway as function of parameters D and T: (a) true detections ($\text{True}_{\#1\text{-}4}$); (b) false detections (Relocated - $\text{True}_{\#1\text{-}4}$).

3.1.2 Experiment 2: Number of Range Bins

In this experiment, the real data were repeatedly processed by algorithm 2 assuming $D = 15$ and $T = 12$, and varying the number of range bins n'_r of the moving window. Once more, only the detections from cars 1-4 were counted as true (i.e., $\text{True}_{\#1\text{-}4}$).

Figure 6 shows the number of detections (all, relocated and true) obtained from each moving window. As it can be seen, the levels increased as the number of range bins n'_r increased, reaching the peak at $n'_r = 512$. In other words, up to this point ($n'_r \leq 512$) the CCM estimation benefited from the increase of training data. Beyond this point ($n'_r > 512$), algorithm 2 lost its robustness against the clutter change over range. As a result, the number of detections (all, relocated and true) started decreasing.

The chosen parameter for algorithm 2 (used for obtaining the results presented in the next sections) was $n'_r = 512$. It is pointed out that the most suitable moving window length depends on the scene and on the motion of the aircraft. Therefore, the parameters chosen in Subsection 3.1 were matched to the experimental data.

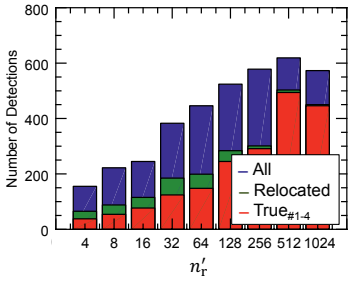

Figure 6: Number of detections as function of the number of range bins n'_r of the moving window ($D = 15$ and $T = 12$).

ISBN 978-3-8007-4636-1 / ISSN 2197-4403

3.2 GMTI Results

The PD STAP detections obtained by algorithms 1 and 2 are shown in **Figure 7**. In this figure, the colors of the detections are related to their absolute ground range velocities. In **Figure 7c**, a detail is shown for algorithm 2 in order to demonstrate the relocation of the true targets to the road axis of the OpenStreetMap (OSM) database [11], carried out by the PD STAP processor with road map information [7-8]. In this figure, the detections are shown before (circles) and after (triangles) relocation, where the center of the runway (white line) was the road axis. The triangles point to the heading angles of the cars and the thin yellow lines connect the PD STAP detections to their closest road points (i.e., on the road axis).

It can be seen from **Figure 7a** that algorithm 1 was not able to detect car 3. Indeed, in this case no training data selection was performed. The full CPI was used as training data (i.e., including moving target signals and strong scatterers), leading to the self-whitening of car 3. In contrast, **Figure 7b** shows that algorithm 2 detected all the cars several times. For instance, it is possible to note car 2 overtaking car 1. In this case, a larger amount of training data was used for the CCM estimation ($L = 39$ CPIs and $n_r' = 512$ range bins) and the moving window took into account the clutter change over range.

Figure 8 shows the eigenvalues distributions (normalized to the noise power) from the training data of both algorithms. For algorithm 1, the eigenvalues distributions exhibited spikes due to the influence of moving target signals and strong scatterers. In contrast, the eigenvalues distributions obtained from algorithm 2 were smooth due to the increased amount of training data. The difference between the first and the second eigenvalues (≈ 15 dB) shows the clutter suppression capability of the PD STAP processor. The fourth eigenvalue is in the noise power level.

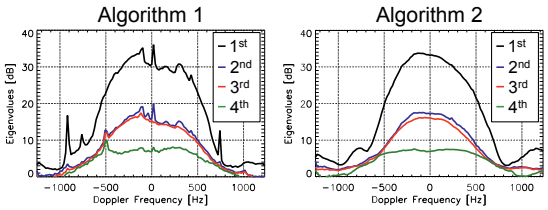

Figure 8: Eigenvalues obtained from the training data in the region of the runway: algorithms 1 and 2.

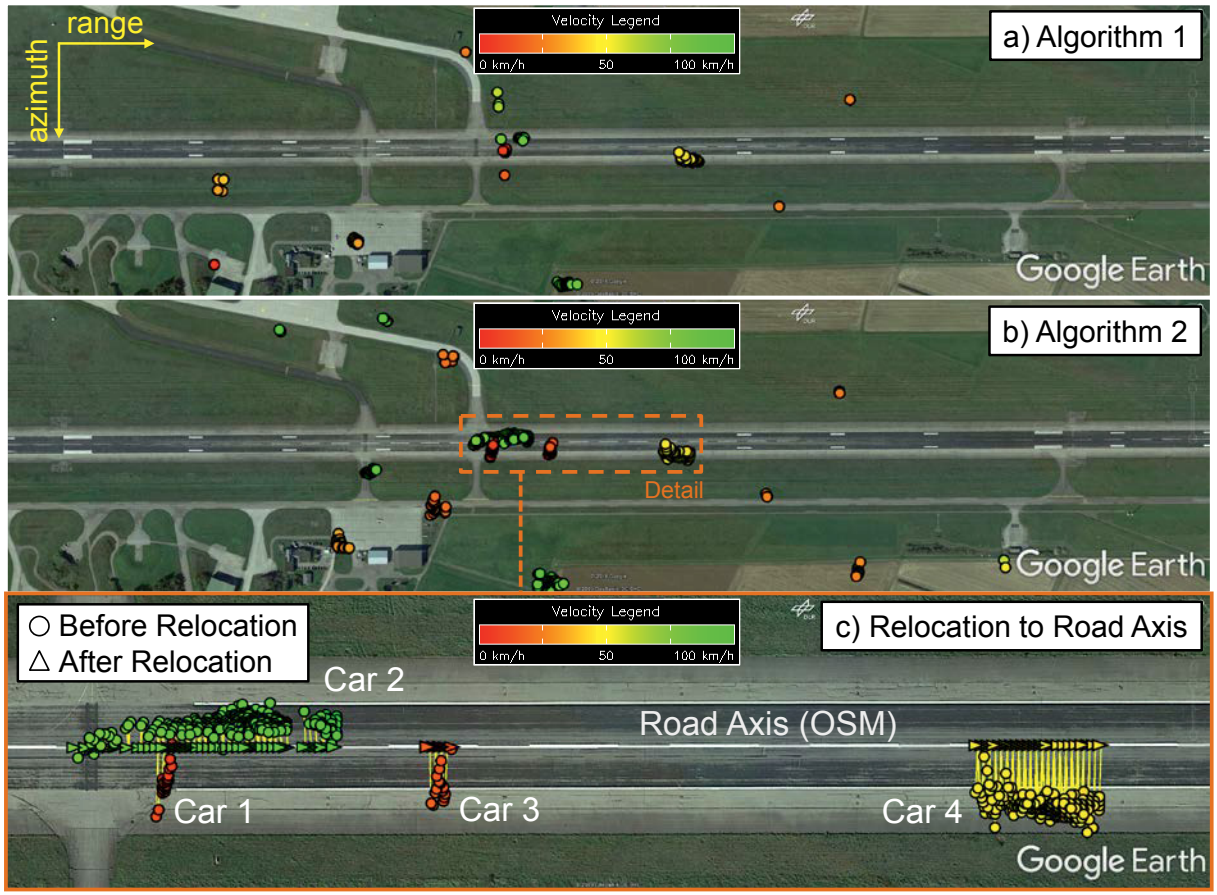

Figure 7: Google Earth images overlaid with PD STAP detections. Algorithms 1 and 2 were applied for selecting the training data for the CCM estimation. The detail shows the relocation of the PD STAP detections (circles) to their nearest OSM road points (triangles) [7-8]. The center of the runway (white line) was the road axis.

ISBN 978-3-8007-4636-1 / ISSN 2197-4403

Figure 9 shows the ground range velocities histograms of the PD STAP detections. This figure allows to compare the amount of false (blue bars) and true detections (red bars) obtained for both algorithms. The true detections ($\text{True}_{\#1\text{-}5}$) could be counted since the positions and the velocities of all cars were known a priori.

It can be seen that a reduced number of detections was obtained by using algorithm 1 and that car 3 was not detected due to the self-whitening. In contrast, much more detections were obtained by algorithm 2. In general, both algorithms presented accurate velocities estimates of the cars, being in very good agreement with those shown in **Figure 4**. The estimated positions were also accurate considering that the cars 1-4 moved on the edges of the runway.

A quantitative comparison between both algorithms is shown in **Table 1**, where it is presented: the numbers of detections (all, relocated and true), the measured probability of false alarm rate $\hat{P}_{\text{fa}}$ and the percentage of true detections relocated to the runway. The $\hat{P}_{\text{fa}}$ was estimated according to:

$$\hat{P}_{\text{fa}} = \frac{\text{All}-\text{True}_{\#1-5}}{N_{\text{a}} N_{\text{r}}}, \qquad (3)$$

where $N_{\text{a}} = 16384$ and $N_{\text{r}} = 1024$ are the numbers of available azimuth and range samples of the experimental data, respectively.

It can be seen from **Table 1** that algorithm 2 obtained nearly seven times more true detections of cars 1-5 ($\text{True}_{\#1\text{-}5}$) than algorithm 1. The $\hat{P}_{\text{fa}}$ increased slightly, whereas $\hat{P}_{\text{fa}} = 5.25 \times 10^{-6}$ is still tolerable. Besides, the last column of the **Table 1** shows the percentage of true detections that remained in the final image (i.e., after applying the road map information). As it can be seen, when algorithm 2 was applied more than 98% of the detections that remained in the final image were true. This value shows the great potential of our PD STAP with the road map information.

The GMTI results presented in this subsection showed that algorithm 2 was able to detect all the cars several times, increasing the number of true detections and keeping a tolerable $\hat{P}_{\text{fa}}$. Algorithm 2 is recommended for both PD STAP processors: with and without road map information. When the road map was used for rejecting the detections that were far from the roads, more than 98% of the detections that remained in the final image were true.

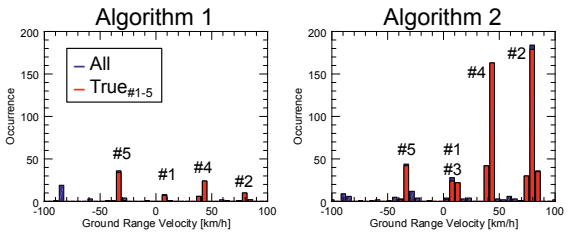

Figure 9: Ground range velocities histograms of the PD STAP detections shown in **Figure 7**: all (blue) and true (red) detections. The detections obtained from cars 1-5 are numbered in the histograms.

Algorithm	All	Rel.	True (#1-4)	True (#1-5)	$\hat{P}_{fa}$ [x10^{-6}]	$\text{True}_{\#1\text{-}4}$/ Rel. [%]
1	134	53	51	77	3.40	96.23
2	625	507	498	537	5.25	98.22

Table 1: Quantitative comparison between algorithms 1 and 2 based on the GMTI results shown in **Figure 7**.

3.3 Real Traffic Scenario

This subsection shows an application example of algorithm 2 in a real traffic scenario. In this case, the PD STAP processor with road map information was applied on a data patch (2048x16384 range-azimuth samples) taken from the large data take shown in **Figure 1a**, where a part of the highway A7 is contained with several moving cars. The parameters of the moving window were: $D = 15$, $T = 12$ and $n'_{\text{r}} = 512$.

Figure 10 shows the GMTI results, where the moving cars are depicted as colored triangles pointing to their heading angles and the OSM road axes of the highway A7 are shown in white. The colors are related to the absolute velocities of the cars on ground. The information box shows some examples of parameters that were obtained for each car on the highway.

Since no ground truth data were available in this experiment, it is not possible to determine the probability of detection, the false alarm rate and the errors of the estimated parameters. Nevertheless, the estimated velocities on the highway A7 were reasonable.

Finally, it can be seen from **Figure 7** and **Figure 10** that the PD STAP processor was able to detect each single car several times, revealing the potential of our GMTI processor for traffic monitoring applications. However, **Figure 10** showed that it is difficult to separate the detections from cars that move close to each other with similar velocity. For this reason, before this processor can be used operationally, a clustering and tracking algorithm needs to be developed.

ISBN 978-3-8007-4636-1 / ISSN 2197-4403

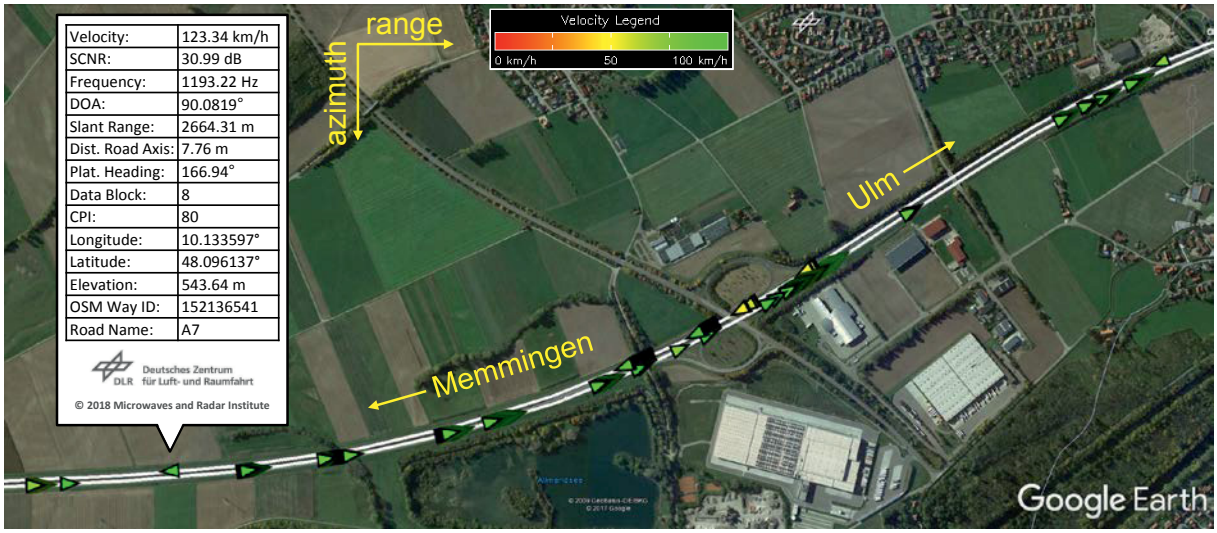

Figure 10: Real traffic in the highway A7. The OSM road axes are shown in white and the cars (triangles) are color coded according to their absolute velocities on the highway. The cars were detected and their parameters were automatically estimated using our PD STAP with road map information [7-8]. Algorithm 2 (proposed in this paper) was used for selecting the training data for the CCM estimation.

4 Conclusions

This paper presents a training data selection algorithm for clutter covariance matrix estimation that can be applied on post-Doppler (PD) STAP processors with and without road map information. The experimental results show that the proposed algorithm outperforms the conventional one (taken as reference) by increasing nearly seven times the number of true detections while keeping a tolerable probability of false alarm rate. For our PD STAP processor with road map information, more than 98% of the detections that remained in the final image were true. Thus, the main goal of the proposed training data selection and update algorithm is fulfilled.

References

[1] W. L. Melvin: "*A STAP overview*," in IEEE Aerospace and Electronic Systems Magazine, vol. 19, no. 1, pp. 19-35, Jan. 2004.

[2] J. R. Guerci: *Space-time adaptive processing for radar*, Artech House, 2014.

[3] F. Gini and M. Rangaswamy: *Knowledge based radar detection, tracking and classification*, vol. 52. John Wiley & Sons, pp.75-101, 2008.

[4] W. L. Melvin and G. A. Showman, "*An approach to knowledge-aided covariance estimation*," IEEE Trans. Aerosp. Electron. Syst., vol. 42, no. 3, pp. 1021–1042, Jul. 2006.

[5] J. H. Bang, W. L. Melvin and G. A. Showman, "*Model-based clutter cancellation based on enhanced knowledge-aided parametric covariance estimation*," IEEE Trans. Aerosp. Electron. Syst., vol. 51, no. 1, pp. 154–166, Jan. 2015.

[6] C. H. Gierull, I. Sikaneta and D. Cerutti-Maori: "*Two-step detector for RADARSAT-2's experimental GMTI mode*," IEEE Trans. Geosci. Remote Sens., vol. 51, no. 1, pp. 436-454, 2013.

[7] A. B. C. da Silva and S. V. Baumgartner: "*Novel post-Doppler STAP with a priori knowledge information for traffic monitoring applications: basic idea and first results*," Advances in Radio Science, vol. 15, pp.77-82, 2017.

[8] A. B. C. da Silva and S. V. Baumgartner: "*STAP moving target position estimation accuracy improvement and false detection recognition using a priori road information*," in Proc. IRS, Prague, Czech Republic, Jun. 2017.

[9] A. Reigber, R. Horn, A. Nottensteiner, P. Prats, R. Scheiber, K.-H. Bethke and S. V. Baumgartner: "*Current status of DLRs new F-SAR sensor*," in Proc. EUSAR, Germany, 2010.

[10] S. V. Baumgartner and G. Krieger: "*Fast GMTI algorithm for traffic monitoring based on a priori knowledge*," IEEE Trans. Geosci. Remote Sens., vol. 50, no. 11, pp. 4626-4641, 2012.

[11] OpenStreetMap-The Free Wiki World Map, Mar. 2018. Available: http://www.openstreetmap.org.